Geophysical Prospecting, 2003, **51**, 169–182

Use of low frequencies for sub-basalt imaging

Anton Ziolkowski,[1]* Peter Hanssen,[2] Robert Gatliff,[2] Helmut Jakubowicz,[3] Andrew Dobson,[1] Gary Hampson,[4] Xiang-Yang Li[2] and Enru Liu[2]

[1]*Department of Geology and Geophysics, University of Edinburgh, West Mains Road, Edinburgh EH9 3JW,* [2]*British Geological Survey, Murchison House, West Mains Road, Edinburgh EH9 3LA,* [3]*Veritas DGC Limited, Crompton Way, Manor Royal Estate, Crawley, West Sussex RH10 2QR, and* [4]*ChevronTexaco UK Limited, 1 Westferry Circus, Canary Wharf, London E14 4HA, UK*

Received June 2002, revision accepted August 2002

ABSTRACT

Many prospective passive ocean margins are covered by large areas of basalts. These basalts are often extremely heterogeneous and scatter the seismic energy of the conventional seismic reflection system so that it becomes difficult to obtain information on deeper reflectors. Since high frequencies are scattered more than low frequencies, we argue that the acquisition system for sub-basalt targets should be modified to emphasize the low frequencies, using much larger airguns, and towing the source and receivers at about 20 m depth. In the summer of 2001 we obtained seismic reflection data over basalt in the northeast Atlantic using a system modified to enhance the low-frequency energy. These new data show deep reflections that are not visible on lines shot in the same places with a conventional system.

INTRODUCTION: WHY SUB-BASALT IMAGING IS IMPORTANT

Large areas of passive ocean margins are covered by basalts, which are often opaque to conventional seismic reflection surveys. For example, the northeast Atlantic margin is a vast, relatively unexplored area – larger than the North Sea – and holds the promise of very large hydrocarbon accumulations. However, in most of this area, the Mesozoic and Palaeozoic sediments that are of interest for hydrocarbon exploration are covered by Cenozoic flood basalts. These basalts are highly heterogeneous, and have many different geometrical characteristics and physical properties. This causes an enormous problem for seismic waves to 'see through' the basalt using conventional towed-streamer technology (e.g. Longshaw, Sunderland and Horn 1998), hence the deep geology of the northeast Atlantic margin is poorly understood. One of the keys to unlocking the huge potential of the margin is to characterize the basalt and find better seismic methods to image beneath it.

*E-mail: anton.ziolkowski@glg.ed.ac.uk

This paper aims to show that the sub-basalt imaging problem can, at least in part, be addressed by obtaining data with sufficient low-frequency energy to enable sub-basalt reflections to be measured with an adequate signal-to-noise ratio. We begin by briefly summarizing previous work on sub-basalt imaging and then look at the characterization of the basalt, particularly in its relation to the propagation of seismic waves. This leads to the conclusion that frequencies well below 30 Hz suffer significantly less attenuation and scattering by the basalt than higher frequencies and, consequently, seismic reflection surveys should be designed to focus on these lower frequencies. We then show how the conventional system may be modified to achieve this. Finally, we show that data shot in 2001, using a system configured to enhance the low-frequency energy, reveals deep reflections that are not visible on earlier data obtained in the same places with a conventional configuration.

PREVIOUS WORK ON SUB-BASALT IMAGING

Various innovative seismic methods have been employed for sub-basalt imaging, including wide-angle seismic surveys, long streamers (up to 12 km), two-boat seismic acquisition,

© 2003 European Association of Geoscientists & Engineers

and multicomponent ocean-bottom surveys (see the extensive list of references in Richardson *et al.* 1999). These efforts have had limited success, but have helped to identify several fundamental problems, including scattering and absorption from rough interfaces, faults and joints, etc., and interference from interbedded units of basalt and sediment. In addition, there are strong sea-surface and 'interbed' multiple reflections that sometimes completely mask deep primary reflections (Longshaw *et al.* 1998).

Wide-angle (i.e. long-offset) seismic surveys, which avoid the scattering problem to some extent, usually give results related only to the large-scale interval velocity of the basalt and not to the reflectivity below (Shipp, Di Nicola-Carena and Singh 1999). Similarly, for some years it appeared that locally converted shear waves, which partially avoid the multiple problem, could offer a 'seismic window' for sub-basalt reflections (Emsley, Boswell and Davis 1998). However, the success of this latter technique is very model-dependent. Furthermore, from an intensive study of real and synthetic data, Hanssen, Li and Ziolkowski (2000) concluded that locally converted shear waves are difficult to use for imaging below the basalt. This suggests that the most likely route to obtaining sub-basalt seismic information remains with non-converted energy.

SEISMIC PROPERTIES OF BASALTS

Many previous studies of the sub-basalt imaging problem have simplistically characterized the basalt as a massive high-velocity slab. Unfortunately, even in relatively simple settings, basalt is often interbedded with thin layers of other lithologies, such as claystone and siltstone (e.g. Gatliff *et al.* 1984). It has been known for many years that the elastic transmission response of a sequence of thin layers is low-pass (O'Doherty and Anstey 1971; Ziolkowski and Fokkema 1986). However, until the work of Mack (1997), it was not generally appreciated that this was relevant to the sub-basalt imaging problem. In particular, Mack performed a 1D seismic modelling experiment to assess the effects of thin-bedded basalt on seismic waves, and concluded that it is important to ensure that the acquisition system can generate and record information at very low frequencies.

The northeast Atlantic basalts also contain lateral heterogeneities and rough interfaces. Modelling studies of wave propagation in heterogeneous media reveal that the medium can be represented by an equivalent homogeneous anisotropic medium for seismic wavelengths an order of magnitude longer than the scale of the heterogeneities (Ebrom *et al.* 1990; Liu, Hudson and Pointer 2000). Field studies of basalts in the northeast Atlantic margin indicate that the basalts are mostly very heterogeneous with scale lengths in the range of tens of metres (Gatliff *et al.* 1984). This is approximately an order of magnitude less than the seismic wavelength for waves with frequencies below 10 Hz. Therefore, the use of low-frequency seismic waves may avoid the scattering problem of thin layering and lateral heterogeneity, and may provide the basis for reflection seismic energy to penetrate through basalt.

Although our main focus and interest is in sub-basalt imaging in the north Atlantic margin, the ideas behind our work have been used on related problems elsewhere. For example, a survey shot in the Indian Ocean in 1991 (Chamot-Rooke *et al.* 1991) showed that low frequencies can be used to profile the Mohorovicic discontinuity beneath the basalt in that area. However, in general, conventional seismic surveys attempt to record a much wider bandwidth than is advocated here. As a result, the low-frequency information can be compromised. Indeed, we believe this to be one of the main reasons for the failure of current seismic methods to obtain sub-basalt information in the north Atlantic. Thus, if it turns out that low frequencies can overcome these problems, this would be of fundamental importance to understanding this area with the seismic method.

MODELLING THE EFFECT OF BASALT ON SEISMIC WAVES

To check the applicability of this approach to the basalts of the north Atlantic margin, we have generated synthetic seismograms to study the effects of thin layering and rough surfaces. To do this we have followed Mack (1997) and modelled wave propagation in horizontally stratified media using the reflectivity method. We used the OSIRIS code (Vilman and Gerstoft 1989) with a model based on real well logs through basalts. Figure 1 shows a log in well 209/9–1 through Palaeocene basalt (Stoker, Hitchen and Graham 1993) and clearly shows that the basalt is extremely heterogeneous. We have modelled the effect of such a composite basalt layer overlying a single deep reflector. Figure 2 shows the one-dimensional earth model we used, in which the water layer was a half-space to eliminate sea-surface multiple reflections, and where there is a single deep reflector at 5025 m. The top of the basalt is at a depth of 1025 m and the basalt is 800 m thick.

Figure 3 shows an offset-dependent synthetic seismogram from this model, where the centre frequency of the source

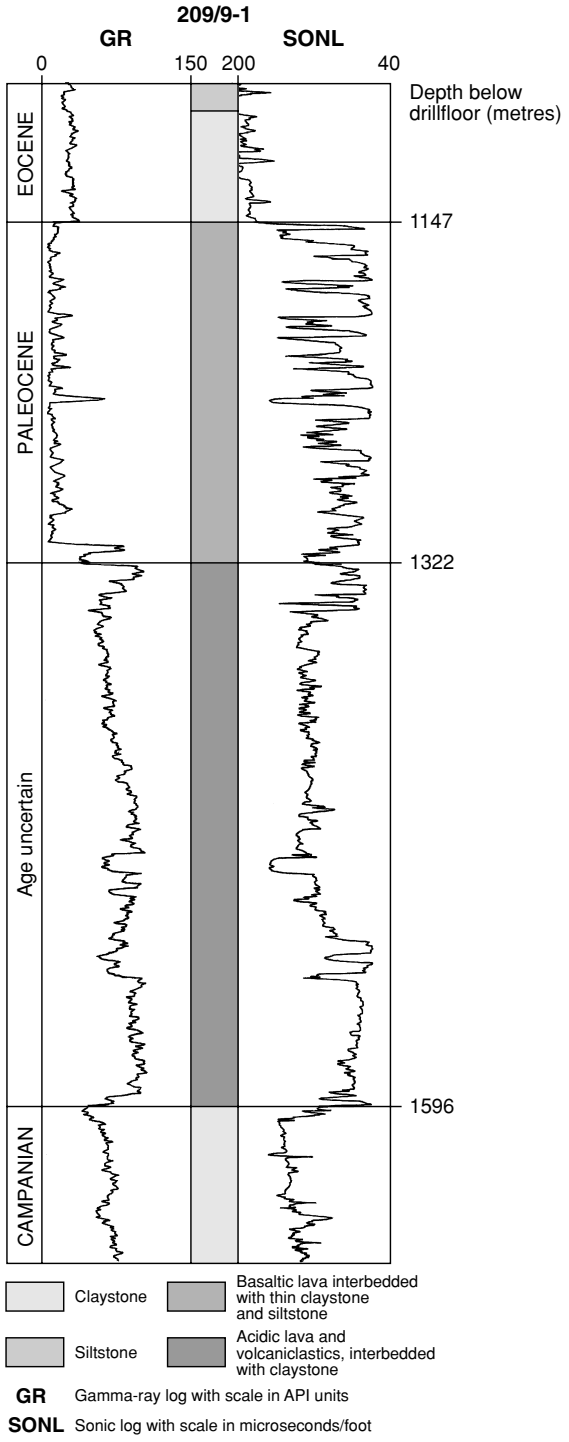

Figure 1 Well logs from basalt north of Shetland.

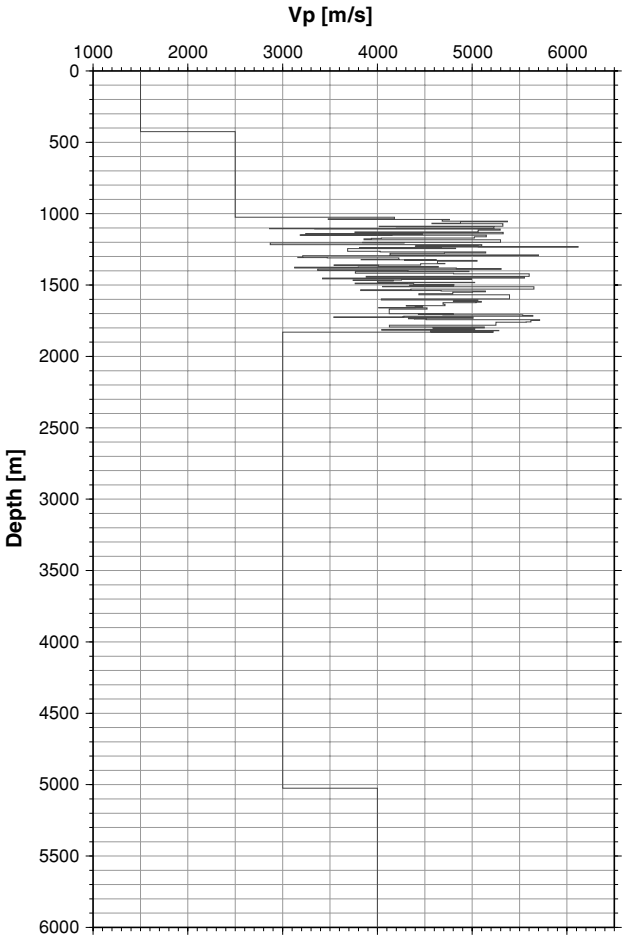

Figure 2 1D earth model for synthetic seismograms showing a very heterogeneous basalt layer at 1000–1820 m and a sub-basalt interface at 5000 m.

time function is 35 Hz, and contrasts this with the response for the same configuration, but with a centre frequency of 10 Hz. The lower frequency clearly shows less scattering in the composite basalt layer and a relatively stronger reflection from the sub-basalt interface at 3.6 s. The amplitude of the deep reflection as a percentage of the amplitude of the top-basalt reflection is plotted as a function of frequency in Fig. 4. It is evident that the attenuating effect of the 800 m thick sequence of basalt and interbedded sediments decreases dramatically as the centre frequency decreases.

In addition to studying the effect of layering on sub-basalt reflections, we have also gone beyond Mack's (1997) work and investigated the effects of a rough interface at the top of the basalt. To do this we have used the boundary-element method (Pedersen, Maupin and Campillo 1996; Pointer, Liu and Hudson 1998). Figure 5 shows the three-layer model used, in which the interface between layer 1 and layer 2 (top basalt) may be rough or smooth. The rough interface was generated using a sine function with a period of 50 m

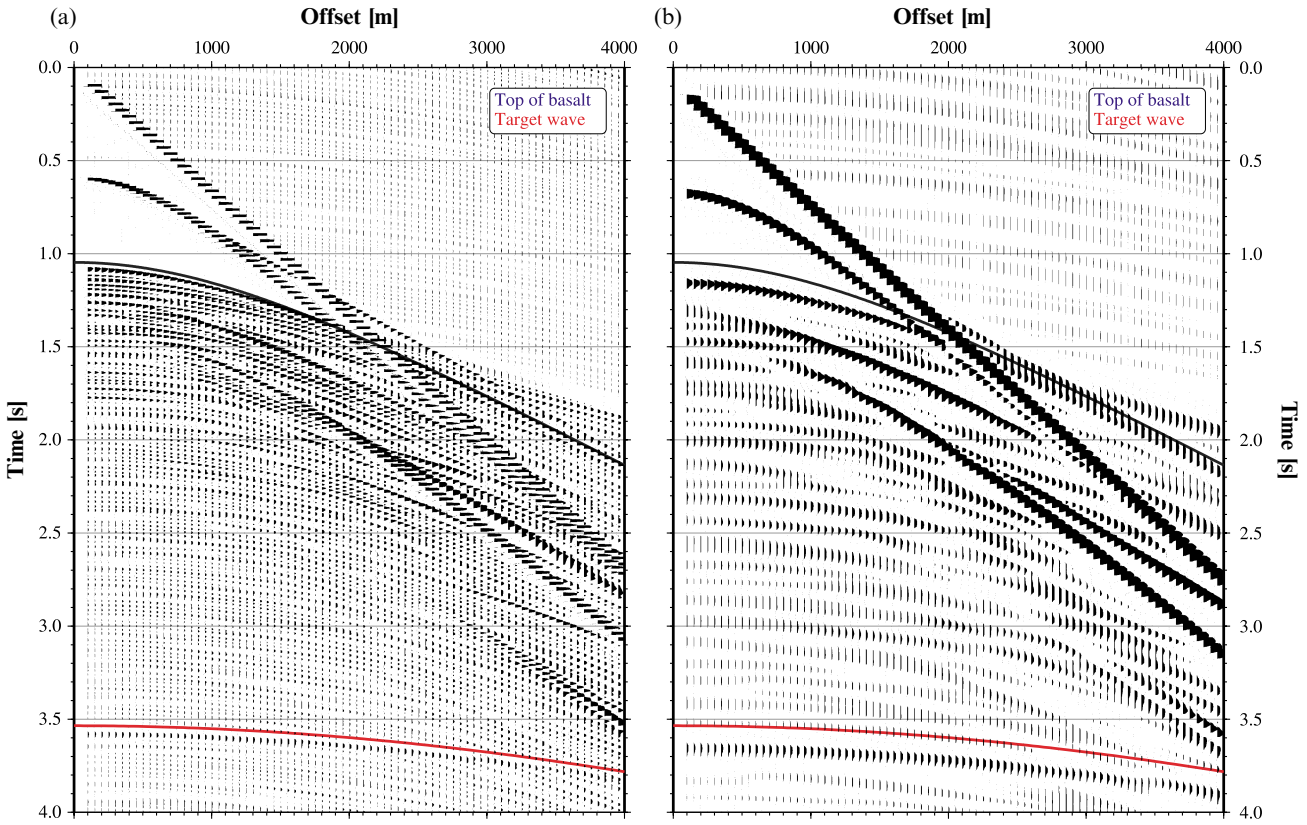

Figure 3 Offset-dependent synthetic seismogram for model of Fig. 2 with (a) 35 Hz source signal (reflection at 3.5 s barely visible) and (b) 10 Hz source signal (reflection at 3.5 s is clearly visible).

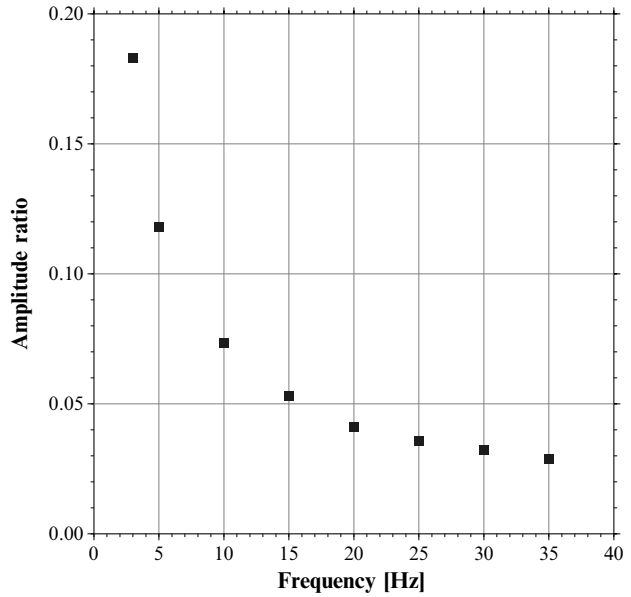

Figure 4 Ratio of amplitude of deep reflector to top-basalt reflection as a function of the centre frequency of the wavelet, for the model shown in Fig. 2.

and an amplitude of 7 m. The period of the sine function was varied randomly by at most 10 m and the amplitude by at most 3 m along its length to make the model slightly more realistic. Layers 1 and 3 are half-spaces with identical physical properties. The source and receivers are located in layer 1, as shown.

Figure 6 shows synthetic seismograms for this configuration and a smooth interface, where the centre frequencies of the source wavelets are 10 Hz and 30 Hz. The results are very similar to what would be computed with the reflectivity method. There are three clear primary reflections: a P-wave reflection off the first interface at about 0.4 s on the nearest trace, a P–S converted-wave reflection off the same interface at about 0.5 s, and a P-wave reflection off the second interface at about 0.65 s. There are also weaker arrivals at later times that are mostly multiple reflections.

Figure 7 show seismograms with the 10 Hz and 30 Hz wavelets for the same model as in Fig. 6, but after the interface has been made rough. The data obtained with the higher-frequency wavelet show a lot of scattering below

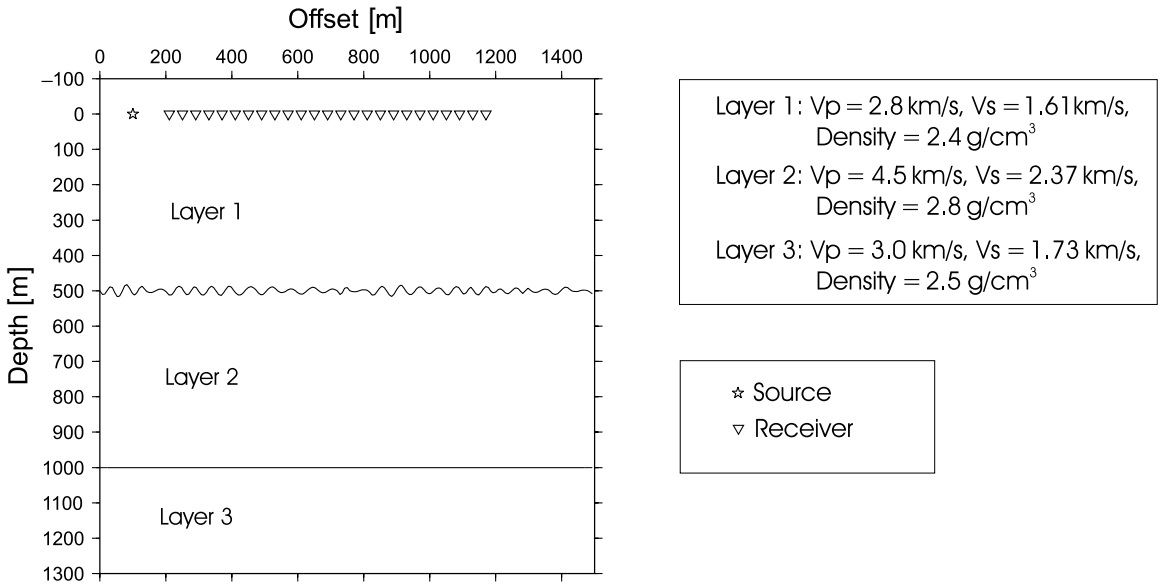

Figure 5 Model for rough surface modelling.

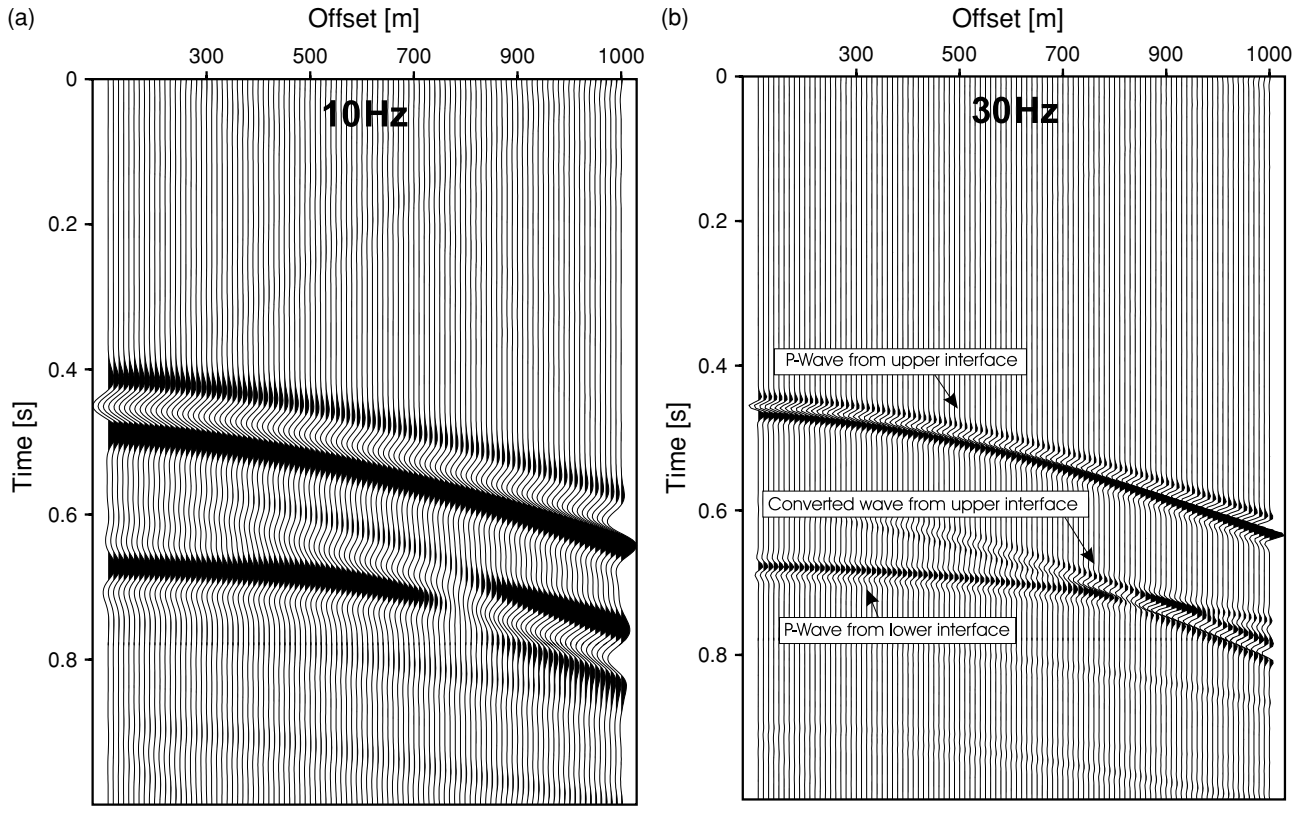

Figure 6 Synthetic seismogram for model in Fig. 5 with first interface smooth and a wavelet with (a) 10 Hz centre frequency and (b) 30 Hz centre frequency.

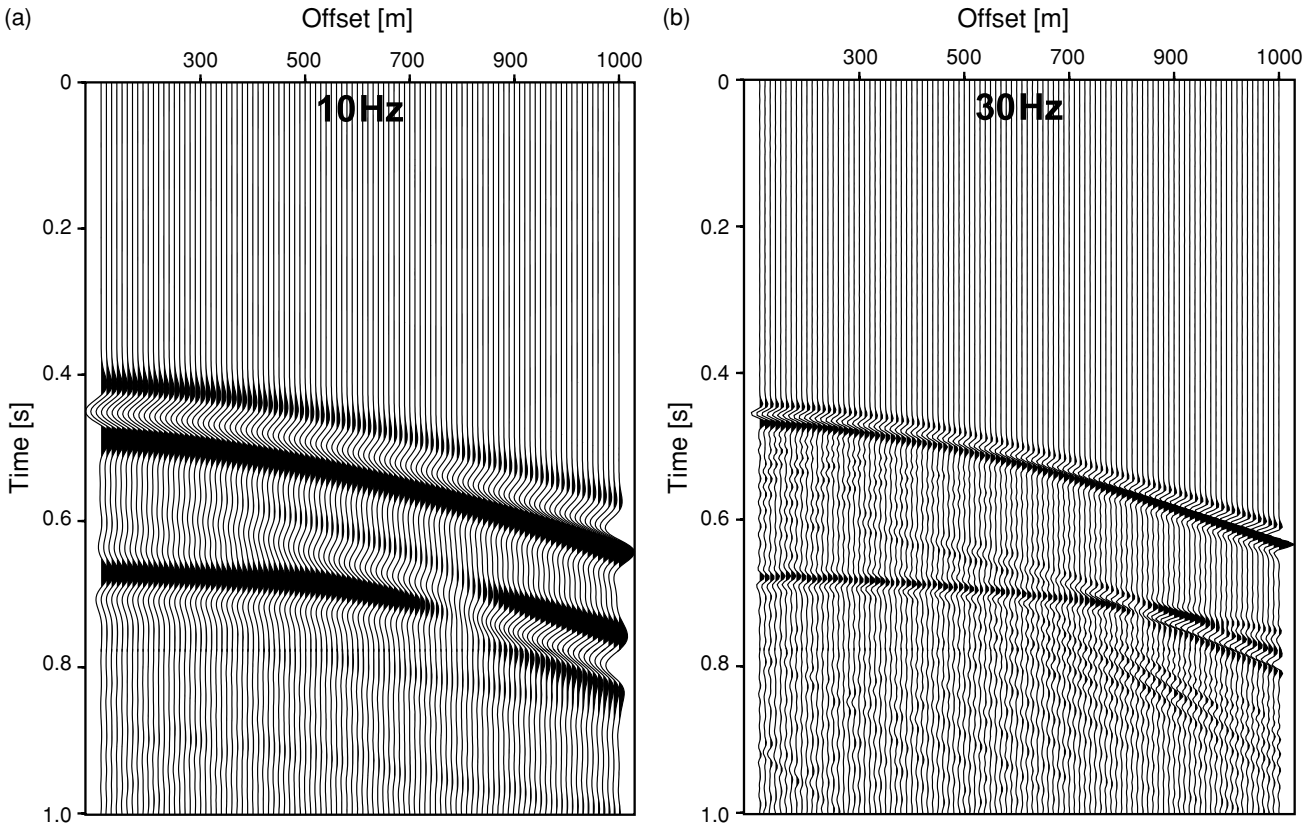

Figure 7 Synthetic seismogram for model in Fig. 5 with first interface rough and a wavelet with (a) 10 Hz centre frequency and (b) 30 Hz centre frequency.

the primary converted wave arrival that breaks up the primary P-wave reflection from the second interface. The 10 Hz wavelet produces much less scattering from this interface. In fact the result is almost identical with the 10 Hz model in Fig. 6, showing that this scale of roughness is essentially invisible at 10 Hz. This is because in this case the wavelength is longer than the scale of the roughness.

The conclusion from this modelling is that scattering from both vertical and horizontal heterogeneities in basalts should be significantly reduced for frequencies below 30 Hz.

DATA ACQUISITION PARAMETERS AND SIGNATURE DECONVOLUTION ISSUES

Effect of the sea-surface reflection

The sea-surface reflection effect in the far-field of a monopole source (or point receiver) is of the form:

$$R(\omega) = 2\sin(\omega D\cos\theta/v), \tag{1}$$

in which ω is the angular frequency, D is the depth of the source (or receiver), θ is the angle of incidence of the downgoing (or upgoing) wave, and v is the velocity of sound in water. The amplitude spectrum of this expression is plotted in Fig. 8. There are notches at

$$\omega = 0,\ \frac{\pi v}{D\cos\theta},\ \frac{2\pi v}{D\cos\theta},\ \cdots\ . \tag{2}$$

The effective bandwidth is between zero and the first notch. Note that the sea-surface reflection can be used to enhance the available bandwidth in the range where the amplitude is greater than unity, that is, in the range

$$\frac{\pi v}{6D\cos\theta} < \omega < \frac{5\pi v}{6D\cos\theta}. \tag{3}$$

The system response is optimized for a given bandwidth and a single monopole source and single receiver by putting the source and receiver at the same depth, when the combined response becomes

$$R_{\mathrm{c}}(\omega) = 4\sin^2(\omega D\cos\theta/v_{\mathrm{w}}). \tag{4}$$

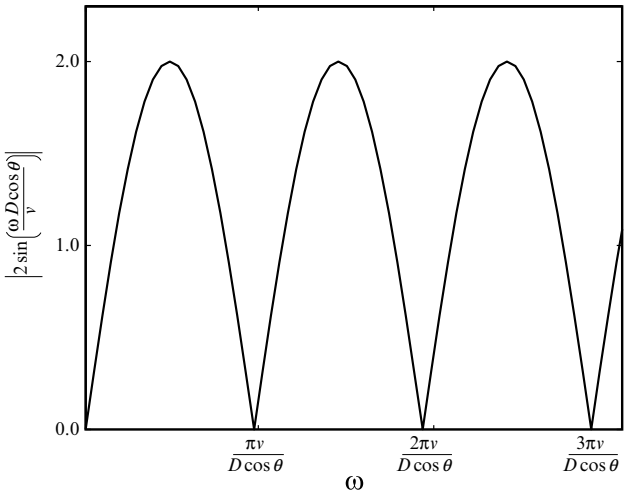

Figure 8 Effect of sea-surface reflection on spectrum of downgoing wave from the source. D is the source depth, θ is the angle of incidence and v is the velocity of sound in water. The horizontal axis is angular frequency. The same effect occurs for an upgoing wave at the receiver.

For example, at normal incidence, $\theta = 0$ and the response is greater than unity over the bandwidth $\pi v/(6D) < \omega < 5\pi v/(6D)$. In conventional seismic reflection surveying, the source and receiver cable depths are typically about 5 m below the sea-surface. For a depth of 5 m, and a velocity of sound in water of 1500 m/s, this effect boosts the amplitude of reflected waves in the bandwidth 30–120 Hz. However, by lowering the source and receiver cable, this effect is moved to lower frequencies. For example, at a depth of 15 m, the optimum bandwidth is shifted to 10–40 Hz. In practice it may be better to tow the source and receiver even deeper, say at 20 m. This would give an optimum bandwidth of 7.5–30 Hz. Unfortunately, although lowering both sources and receivers can certainly be used to exploit the sea-surface reflection and enhance low frequencies, there are other effects that counteract this and also need to be taken into account. For example, Hobbs and Snyder (1992) reported on the source–receiver geometry used by BIRPS (British Institutions Reflection Profiling Syndicate) for deep seismic reflection profiling over the previous 10 years. In the BIRPS configuration, the receivers were towed relatively deep, typically at 15 m, and produced a corresponding notch in the spectrum of the received wavelet at 50 Hz. However, the source signatures reported in the paper are for a source depth of 7.5 m, and therefore introduce a notch into the downgoing wavelet at 100 Hz. As a result, the BIRPS system was only partially optimized for maximum energy in the desired low-frequency bandwidth. Indeed, Hobbs and Snyder (1992) did consider towing the source deeper, but apparently decided against it. It is worth quoting the relevant section of their paper: 'Early testing of tow depth revealed the importance of the surface ghost in producing a notch at the higher frequency range [their fig. 4]. In changing the tow depth of the source from 7.5 m to 10 m, the high-frequency notch moves down from 100 Hz to 75 Hz and beneficially augments the amplitude of the low-frequency component of the signal. However, detailed analysis shows that the period of the bubble pulse has marginally decreased because of the increased hydrostatic pressure'. This is an important point and is considered below.

The effect of depth on airgun bubble oscillations

In a normal airgun array the largest gun has a volume not greater than about 7.4 l (465 cu. in.). At a depth of 5 m, and a pressure of 135 bar (2000 psi), a 7.4 l gun emits an air bubble which oscillates with a period of about 130 ms, corresponding to a fundamental frequency of 7.7 Hz, as shown in Fig. 9. The bubble oscillation period T is given approximately by the modified Rayleigh–Willis formula:

$$T = k\,\frac{P^{1/3}\,V^{1/3}}{(P_{\mathrm{atm}} + \rho\,\mathrm{g}\,D)^{5/6}}, \qquad (5)$$

where P is the gun pressure, V is the gun volume, P_{atm} is atmospheric pressure, ρ is the density of water, g is gravitational acceleration, D is the depth of the gun, and k is a constant whose value depends on the units. From the bubble period for one gun of known volume, pressure, depth, and bubble period, it is possible to determine the constant k, and hence to determine the bubble period of any gun of known volume, pressure and depth. For example, a 7.4 l gun at a depth of 15 m would have a bubble period of about 85 ms, corresponding to a fundamental frequency of about 11.7 Hz.

Since airguns are already operated at close to the maximum safe pressure, the only parameters that can be adjusted to control their output are the depths and volumes of air discharged. Unfortunately, in accordance with the modified Rayleigh–Willis relationship, lowering an airgun decreases the time period of the bubble (as noted by Hobbs and Snyder 1992), and therefore increases the frequency generated by the gun. For example, if a conventional airgun array is put at 15 m, instead of its normal depth of 5 m, the frequency of oscillation of every bubble in the array is increased by about 50%. Thus, the volumes of the guns must be

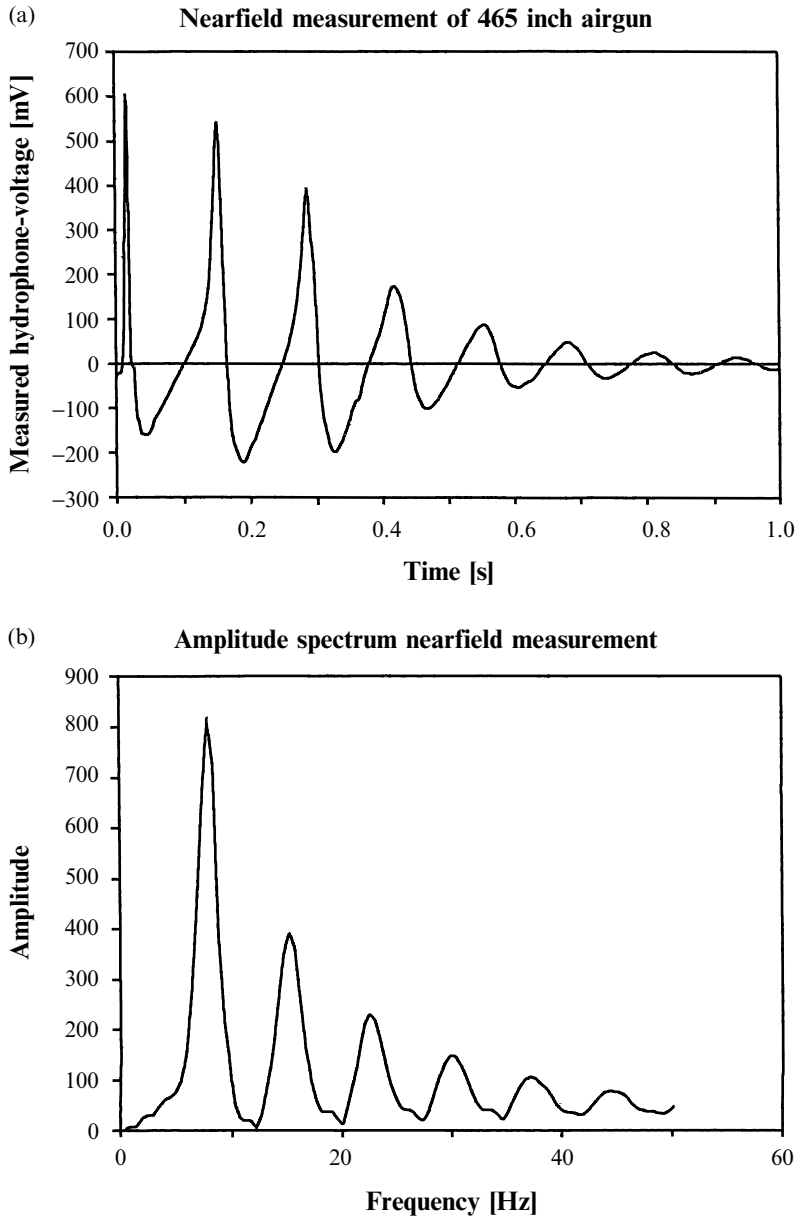

Figure 9 (a) Measured voltage output of an uncalibrated hydrophone 1 m from a 465 cu. in. airgun at a depth of 5 m, firing at a pressure of 135 bar (2000 psi); (b) shows the amplitude spectrum of (a) in arbitrary units.

increased. However, because the period depends on the cube root of the gun volume, the increase must be substantial. For example, a 2000 cu. in. airgun at 17 m and 135 bar (2000 psi) would have a bubble period of about 130 ms, corresponding to a fundamental frequency of about 7.7 Hz. That is, a 2000 cu. in. gun at 17 m has the same fundamental frequency as a 465 cu. in. gun at 5 m, as illustrated in Fig. 10.

In practice it is not necessary to put all the guns at the same depth. If each gun is put at a depth at which its sea-surface reflection arrives half a bubble period after the direct wave, this optimizes the energy that the bubble can deliver (Ziolkowski 1971). That is, to optimize the downgoing energy from an airgun, we require

$$D = \frac{vT}{4} = \frac{\lambda}{4}, \tag{6}$$

where λ is the wavelength corresponding to the bubble period T. We believe this idea was first used in the discovery of the sedimentary basin on Rockall Plateau in 1969 by Roberts *et al.* (1970), where a single 30 cu. in. airgun was towed at

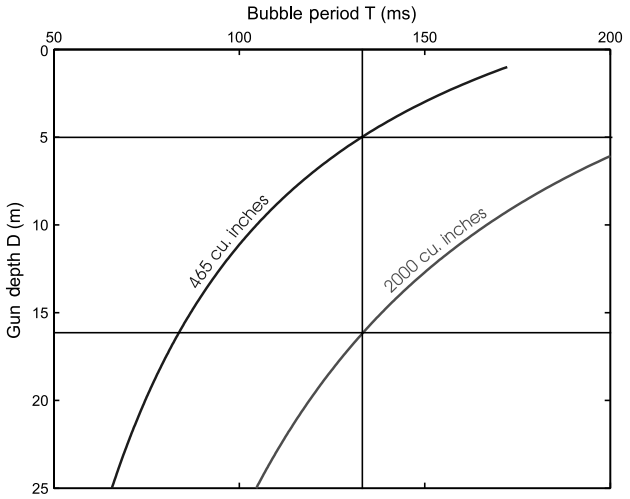

Figure 10 Bubble period as a function of depth for two airguns of volumes 465 and 2000 cu. in., calculated using the modified Rayleigh–Willis formula and the single data point provided by the measurement shown in Fig. 9.

15 m, and a single-channel hydrophone streamer was also towed at 15 m. Incidentally, the survey was shot in a gale and, although it is never desirable to acquire data in severe weather conditions, an additional advantage of lowering both the source and the streamer is that noise due to surface conditions is considerably reduced.

By combining (5) and (6) and eliminating the bubble period T, the optimum depth of any gun of volume V and firing pressure P can be found. Additional options are available with clustering of airguns.

In contrast to using larger gun volumes at depth, Avedik *et al*. (1993) suggested tuning the airgun array for maximum low-frequency energy rather than for the maximum primary-to-bubble ratio used as the conventional design criterion. They worked within the constraints of the rather limited compressor capacity of IFREMER (Institut Francais de Recherche pour l'Exploitation de la Mer) vessels and existing airgun sizes. Adopting the idea of an optimum depth (Ziolkowski 1971), they towed the guns deep and arranged the gun firing times such that the first bubble collapse of each of the different airgun bubbles occurred at the same time. This produced a long oscillating signal with high energy and a rather narrow spectrum that is roughly one octave wide at −6 dB points and with the lowest frequency in this bandwidth not less than 20 Hz (see, for example, their figs 7 and 15). Although we have not pursued this route ourselves, it demonstrates that there are other avenues for enhancing low frequencies, including varying the timing of individual guns.

Finally, it is important to note that the resolution provided by any low-frequency source is inherently less than with a conventional broadband configuration. In the case of the sub-basalt problem, this is perhaps a small price to pay for the ability to have at least some signal in the recording. However, it is still desirable to maximize the resolution that is available through appropriate acquisition and processing techniques. In particular, we advocate that the source signature be compressed to a shorter, more desirable signal through deconvolution using a measured signature. Details of techniques that can be used to provide the measured signatures can be found, for example, in Ziolkowski *et al*. (1982) and Hobbs and Jakubowicz (2000).

RESULTS

In 2001 these ideas were implemented in surveys over the north Atlantic margin basalt recorded by Veritas DGC. The normal airgun array was modified to include much larger airguns and towed at 15 m. A solid streamer was used at a depth also of 15 m. Some of the data were acquired along the same profiles as seismic lines shot earlier with a conventional configuration. We show lines from two areas.

The first area focused on UK Blocks 213/5 and 214/1 with the 1997 and 2001 lines orientated in a SE–NW direction, straddling the UK-Faeroes line. Figure 11 compares data from the conventional and the low-frequency configurations for a pair of lines in this area. The data processing on both sections was identical and included dip-moveout and prestack time migration. The 2001 (low-frequency) line shows stronger reflections below the top of basalt that can be more readily identified than in the case of the older data obtained with the conventional acquisition configuration. Normalized spectra extracted from the data, shown in Fig. 12, also show that the 2001 line has enhanced low-frequency energy, as expected.

Figure 13 compares a 1998 line with data obtained in 2001 with a low-frequency configuration in the same location in the Faeroes area. The two datasets have been processed with equivalent sequences, including prestack depth migration, and have been converted back to time. The top basalt reflection lies between 1.5 s and 2 s on the left of the sections, before dipping down to 3 s on the right-hand side. The low-frequency data provide a much clearer picture of the geology beneath the basalt and allow at least speculative interpretation of the base basalt reflection, presenting a clearer picture of the deeper structures.

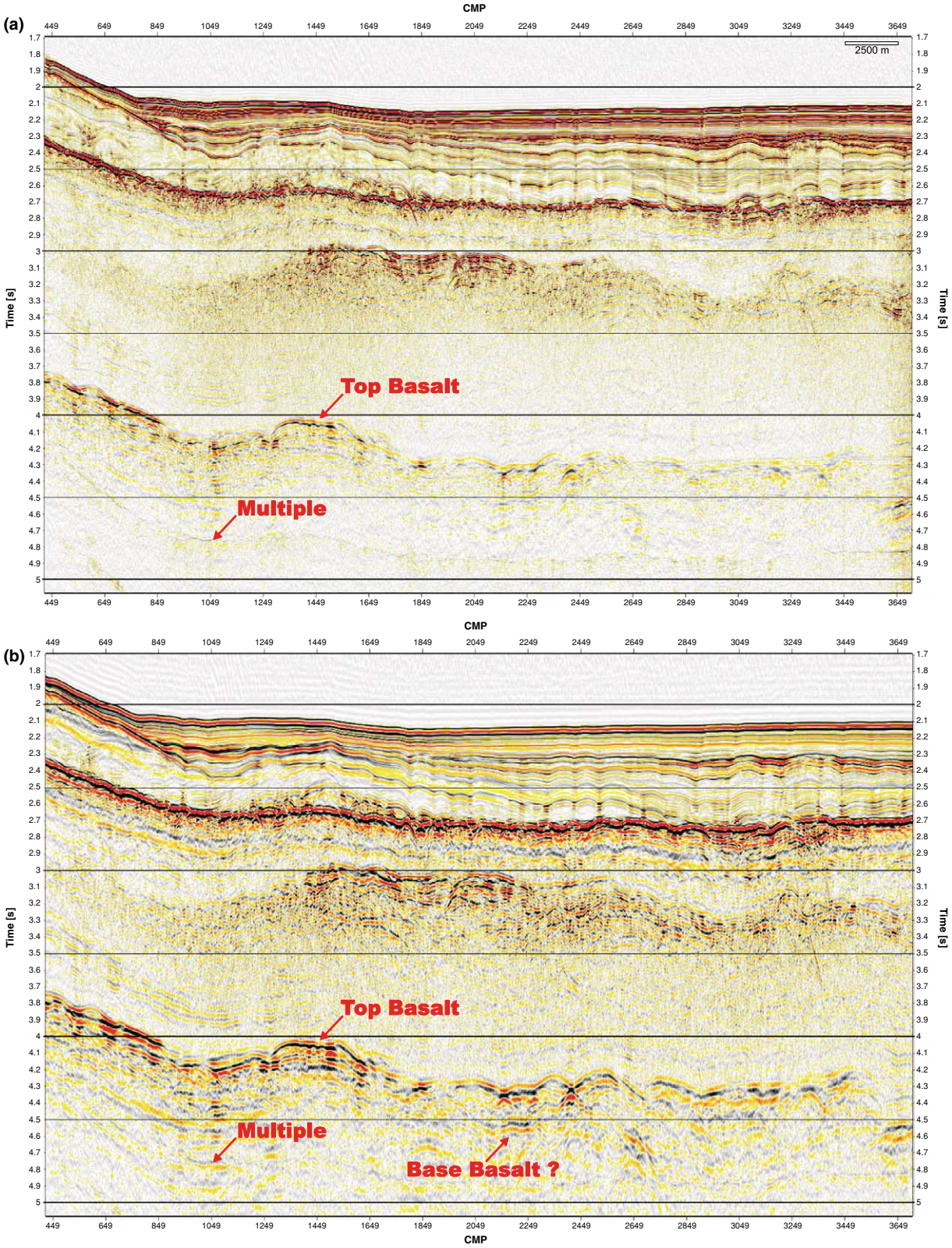

Figure 11 Comparison of (a) 1997 line, shot on northeast Atlantic margin with conventional seismic reflection system, with (b) low-frequency line, shot in similar location in 2001.

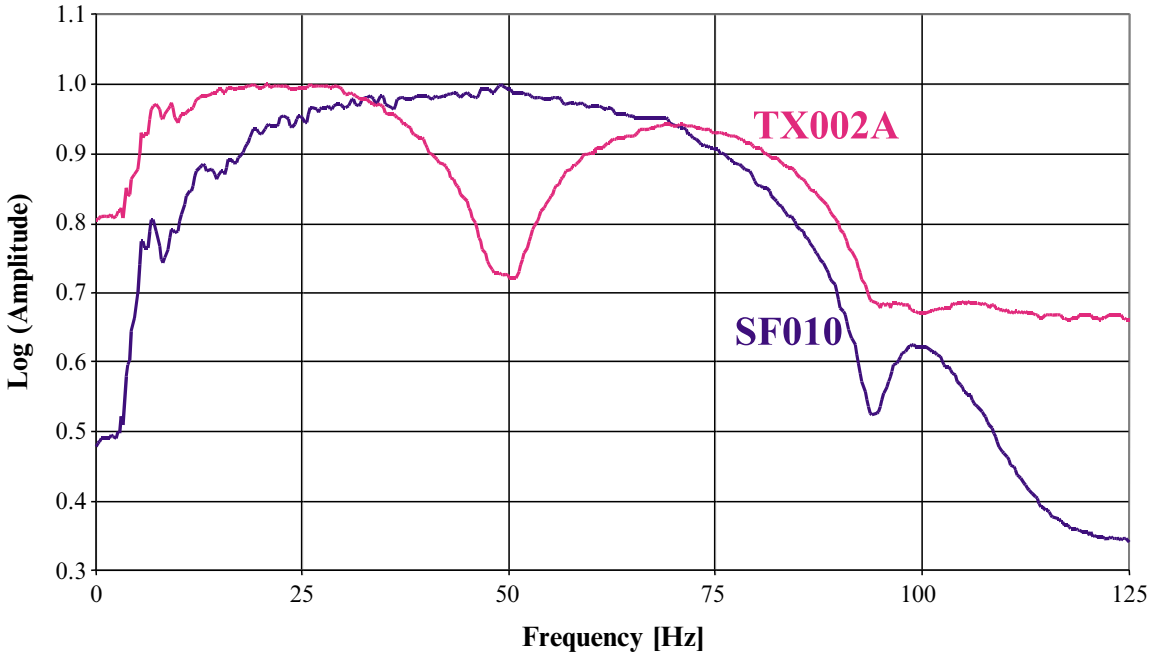

Figure 12 Normalized spectra from the two lines shown in Fig. 11. The 1997 line was shot with the shallower source and receiver and has the first notch at about 90 Hz, indicating a source or receiver depth of about 8 m. The 2001 line was shot with source and receiver depths of 15 m, putting the first notch at 50 Hz. The 2001 line has much greater low-frequency content.

Figure 14 shows a comparison similar to that in Fig. 13, but from a second line in the Faeroes area. In this case, the basalt thins from the left-hand side of the lines, and it is noticeable that the data quality of the deep data improves towards the right-hand side on both sections. However, the new data show an event between 3.5 s and 4 s on the left-hand side that dips upwards from left to right, and is antithetic to any shallow reflections. This event is unlikely to be a multiple, and provides strong evidence for the superior penetration in the low-frequency result. In addition, the low-frequency data also show a number of other features beneath the basalt that are absent on the conventional section, and provide a more reliable starting point for interpretation than do the conventional data.

CONCLUSIONS

Large areas of passive ocean margins are covered by basalts that may conceal enormous reserves of hydrocarbons. Various innovative seismic methods have been employed for sub-basalt imaging, but they have had limited success. The passive ocean margin basalts are very heterogeneous and scatter high frequencies more than low frequencies. To increase the probability of obtaining detectable sub-basalt reflections, it is essential to design the seismic reflection system to emphasize the low frequencies. The source and receiver must be towed deep (about 20 m) and much larger airguns than normal must be used: an increase in volume by at least a factor of 5. Data obtained with larger airguns towed at 15 m and with the streamer at the same depth show improved deep reflections below the top of the basalt.

Although we hope the results presented in this paper help to establish and confirm that low frequencies are a key that can be used to reveal information from sub-basalt reflectors, there remains much work to be done. This includes developing new source arrays and acquisition configurations that would provide even more energy in the desired bandwidth. In particular, Sonneland *et al.* (1986) showed how two or more streamers towed at different depths can be used to eliminate the ghost notch at the receiver side, thus increasing the bandwidth of the received signal, while Singh, Hobbs and Snyder (1996) used the same idea and produced very good results. Indeed, it should also be feasible to alternate between a shallow (high-frequency) and deep (low-frequency) source so that the low-frequency results do not compromise the availability of broadband data from shallower objectives. Similarly, the spatial sampling considerations for low frequencies would

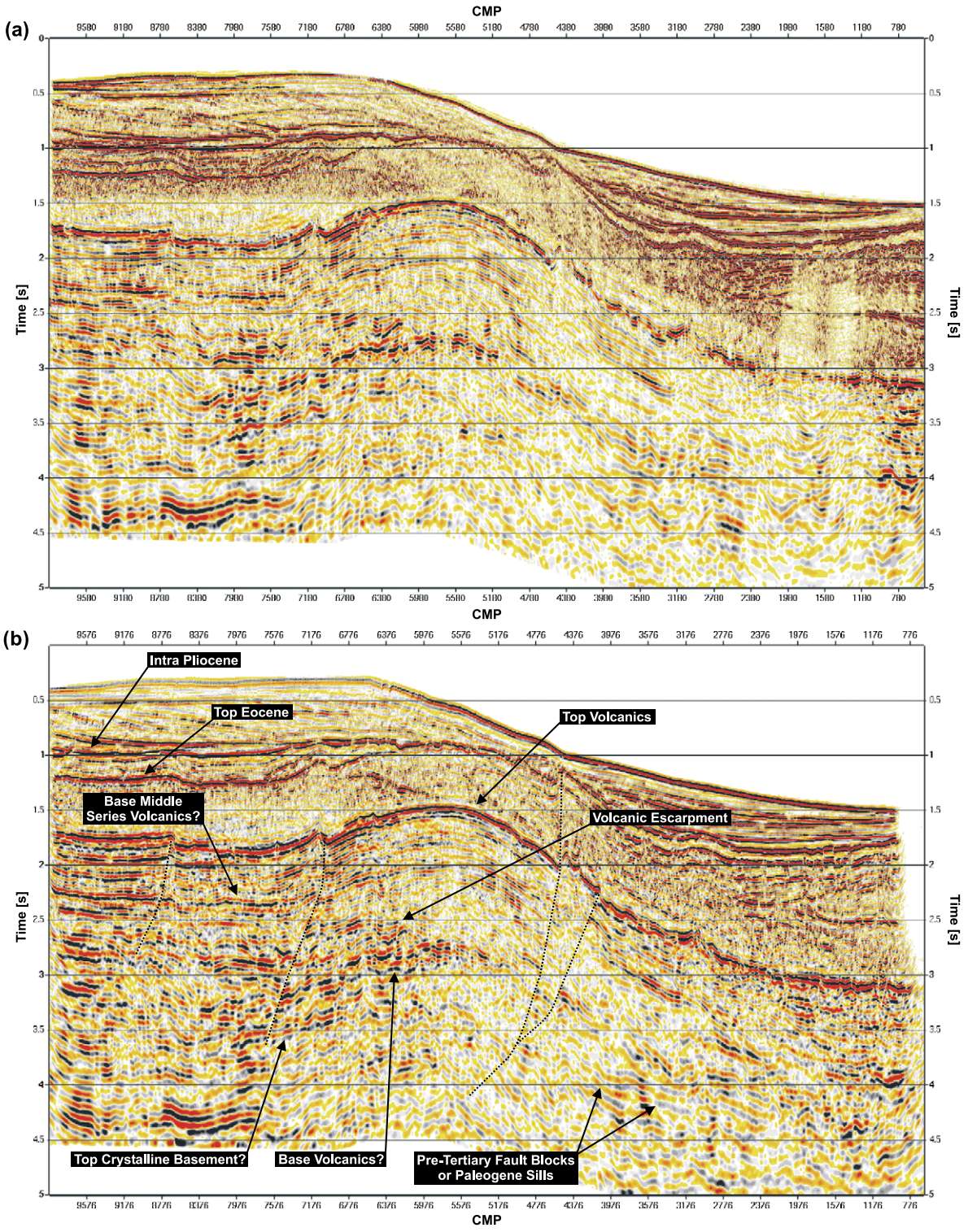

Figure 13 Prestack depth migration (displayed in time) of (a) 1998 data, obtained with conventional acquisition configuration, compared with (b) lower-frequency configuration 2001 data. For comparison purposes the fold of the 2001 data was restricted to match that of the 1998 data. The two data sets were processed with equivalent parameters and offset ranges, and were also migrated with the same depth model.

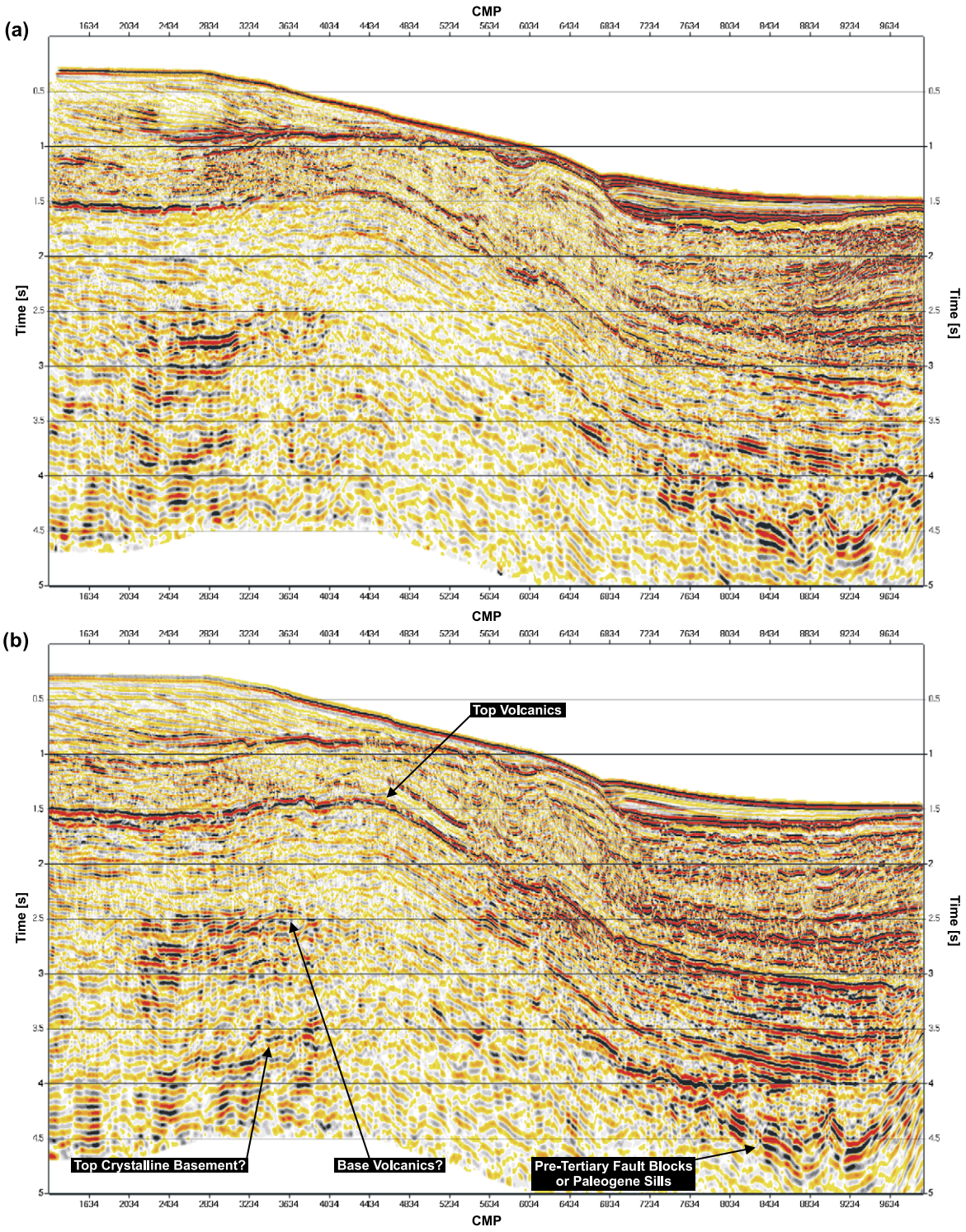

Figure 14 Prestack depth migration (displayed in time) of (a) 1997 data, obtained with conventional acquisition configuration, compared with (b) lower-frequency configuration 2001 data.

reduce the (cross-line) effort required for a 3D survey. This is important because 3D effects are also likely to be critical for successful sub-basalt imaging. We are therefore currently pursuing these and other ideas with a view to enhancing further our ability to obtain information from sub-basalt reflectors.

ACKNOWLEDGEMENTS

A.Z. thanks Harry Mack for interesting discussions. We are grateful to ChevronTexaco and the BLAST Group (Anadarko, Statoil, Enterprise Oil, Phillips, Veba Oil, and Veritas DGC) for allowing us to show data from the north Atlantic margin, and to David Wright for help with Figs 8 and 10. We also thank the anonymous reviewers for their positive comments and suggestions for improving the paper. This paper is published with the approval of the Executive Director of the British Geological Survey.

REFERENCES

Avedik F., Renard V., Allenou J.P. and Morvan P. 1993. 'Single bubble' air-gun array for deep exploration. *Geophysics* **58**, 366–382.

Chamot-Rooke N., de Voogd B., Diebold J., Dyment J., Farcy F., Fleitout L. *et al.* 1991. Seismic reflection profiling across the central Indian Ocean deformed lithosphere. *EOS, Transactions of the American Geophysical Union*, Fall Meeting, 9–13 December, San Francisco, USA, p. 488.

Ebrom D., Tatham R., Sekharan K.K., McDonald J. and Gardner G.H.F. 1990. Dispersion and anisotropy in laminated versus fractured media: an experimental comparison. 60th SEG meeting, San Francisco, USA, Expanded Abstracts, 1416–1419.

Emsley D., Boswell P. and Davis P. 1998. Sub-basaltic imaging using long offset seismic data. 60th EAGE conference, Leipzig, Germany, Extended Abstracts, Paper 1–48.

Gatliff R.W., Hitchen K., Ritchie J.D. and Smythe D.K. 1984. Internal structure of the Erlend Tertiary volcanic complex, north of Shetland, revealed by seismic reflection. *Journal of the Geological Society* **141**, 555–562.

Hanssen P., Li X.-Y. and Ziolkowski A. 2000. Converted waves for sub-basalt imaging? 70th SEG meeting, Calgary, Canada, Expanded Abstracts, 1174–1177.

Hobbs R. and Jakubowicz H. 2000. Marine source signature measurement using a reference seismic source. 70th SEG meeting, Calgary, Canada, Expanded Abstracts, 57–60.

Hobbs R. and Snyder D. 1992. Marine seismic sources for deep seismic reflection profiling. *First Break* **10**, 417–426.

Liu E., Hudson J.A. and Pointer T. 2000. Equivalent medium representation of fractured rocks. *Journal of Geophysical Research* **105**, 2981–3000.

Longshaw S.K., Sunderland J. and Horn I. 1998. Mode conversion and multiples. 68th SEG meeting, New Orleans, USA, Expanded Abstracts, 1340–1342.

Mack H. 1997. Seismic response of Tertiary basalt flows in Northeast Atlantic – a modelling study. 59th EAGE conference, Geneva, Switzerland, Extended Abstracts, Paper B017.

O'Doherty R.F. and Anstey N.A. 1971. Reflections on amplitudes. *Geophysical Prospecting* **19**, 430–458.

Pedersen H.A., Maupin V. and Campillo M. 1996. Wave diffraction in multilayered media with the Indirect Boundary Element Method: application to 3-D diffraction of the long-period surface waves by 2-D lithospheric structures. *Geophysical Journal International* **125**, 545–558.

Pointer T., Liu E. and Hudson J.A. 1998. Numerical modelling of seismic waves scattered by hydrofractures: application of the indirect boundary element method. *Geophysical Journal International* **135**, 289–303.

Richardson K.R., White R.S., England R.W. and Fruehn J. 1999. Crustal structure east of the Faroe Islands: mapping sub-basalt sediments using wide-angle seismic data. *Petroleum Geoscience* **5**, 161–172.

Roberts D.G., Bishop D.G., Laughton A.S., Ziolkowski A.M., Scrutton R.A. and Matthews D.H. 1970. New sedimentary basin on Rockall Plateau. *Nature* **225**, 170–172.

Shipp R., Di Nicola-Carena E. and Singh S. 1999. 2-D full wavefield inversion of wide angle real marine seismic data. 69th SEG meeting, Houston, USA, Expanded Abstracts, 1394–1397.

Singh S., Hobbs R. and Snyder D. 1996. Broadband receiver response from dual-streamer data and applications in deep reflection seismology. *Geophysics* **61**, 232–243.

Sonneland L., Berg L.E., Eidsvig P., Haugen A., Fotland B. and Vestby J. 1986. 2-D deghosting using vertical receiver arrays. 56th SEG meeting, Houston, USA, Expanded Abstracts, Session S11.6.

Stoker M.S., Hitchen K. and Graham C.C. 1993. *The Geology of the Hebrides and West Shetland Shelves, and Adjacent Deep-Water Areas*. HMSO, London.

Vilman O. and Gerstoft P. 1989. *High-Speed Forward Modelling Applied in Seismic Data Processing*. Report 89.238, Odegaard A/S, Copenhagen.

Ziolkowski A.M. 1971. Design of a marine seismic reflection profiling system using airguns as sound source. *Geophysical Journal of the Royal Astronomical Society* **23**, 499–530.

Ziolkowski A. and Fokkema J.T. 1986. Tutorial: the progressive attenuation of high-frequency energy in seismic reflection data. *Geophysical Prospecting* **34**, 981–1001.

Ziolkowski A.M., Parkes G.E., Hatton L. and Haugland T. 1982. The signature of an airgun array: computation from near-field measurements including interactions. *Geophysics* **47**, 1413–1421.